

Individual Control and Readout of Qubits in a Sub-Diffraction Volume

Eric Bersin,^{1,*} Michael Walsh,^{1,*} Sara L. Mouradian,¹ Matthew E. Trusheim,¹ Tim Schröder,^{1,†} and Dirk Englund^{1,‡}

¹*Department of Electrical Engineering and Computer Science,
Massachusetts Institute of Technology, Cambridge, Massachusetts 02139, USA*

Medium-scale ensembles of coupled qubits offer a platform for near-term quantum technologies including computing [1], sensing [2], and the study of mesoscopic quantum systems [3–5]. Atom-like emitters in solids [6] have emerged as promising quantum memories, with demonstrations of spin-spin entanglement by optical [7] and magnetic [8] interactions. Magnetic coupling in particular is attractive for efficient and deterministic entanglement gates, but raises the problem of individual spin addressing at the necessary nanometer-scale separation. Current super-resolution techniques [9, 10] can reach this resolution, but are destructive to the states of nearby qubits. Here, we demonstrate the measurement of individual qubit states in a sub-diffraction cluster by selectively exciting spectrally distinguishable nitrogen vacancy (NV) centers [11]. We demonstrate super-resolution localization of single centers with nanometer spatial resolution, as well as individual control and readout of spin populations. These measurements indicate a readout-induced crosstalk on non-addressed qubits below 4×10^{-2} . This approach opens the door to high-speed control and measurement of qubit registers in mesoscopic spin clusters, with applications ranging from entanglement-enhanced sensors [12] to error-corrected qubit registers [13, 14] to multiplexed quantum repeater nodes [15, 16].

Major advances towards larger coherent spin systems in diamond have recently been made by controlling nuclear spins [17] or dark electron spins [18] through one NV center and by coupling electron spins of two NV centers [8]. These advances suggest that a system of strongly coupled color centers, each coupled to proximal dark spins, could provide a scalable platform for controlled spin-spin interactions, as illustrated in Figure 1a.

A central challenge for coherent control of such multi-spin systems is the ability to measure individual NV centers without collapsing the states of nearby NVs. Here we address this problem by making use of the inhomogeneous distribution of NV center optical transitions, attributed to natural and defect-induced lattice strain [19, 20]. The strain field $\vec{\sigma}$ enters the excited state Hamiltonian as $H_{\text{strain}} = \vec{\sigma} \cdot \vec{V}$ [21], where \vec{V} is the vector of orbital operators, and can be divided into axial and transverse components, with differing effects detailed in Figure 1b. We find that this distribution persists even for closely-spaced NV centers, allowing us to optically address individual emitters within a diffraction-limited volume.

We investigate this approach to multi-qubit readout in a Type IIa polycrystalline diamond (PCD, see Methods). The scanning confocal image in Figure 1c shows NV centers in one domain of this PCD near a gold stripline for microwave delivery that cuts across a grain boundary, visible as the bright strip in the image. Despite the high strain of the PCD [22], its low nitrogen content allows for NVs with coherence times exceeding 200 μs [23] at room temperature. The histogram of the NV optical transitions (Figure 1d) indicates an inhomogeneous distribu-

tion with standard deviation of 294 GHz, nearly 5 times broader than what we measure in single-crystal diamond samples [23].

This broad inhomogeneous distribution allows us to spectrally distinguish NVs below the diffraction limit. Figure 1e shows a photoluminescence excitation (PLE) spectrum taken on a representative fluorescence site on the sample, labeled site 1 in the inset of Figure 1c. The spectrum reveals several distinct zero-phonon line (ZPL) peaks, indicative of the presence of multiple NV centers within the diffraction-limited spot. Spatially scanning a narrow laser resonant with one of the transitions in Figure 1e preferentially induces fluorescence from a single NV center, selectively imaging this defect out of the cluster. Performing this scan for each observed transition, we find that they correspond to only three spatial positions. Second-order autocorrelation and optically detected magnetic resonance (ODMR) measurements further confirm the presence of three NV centers in this site [23]. The most prominent and well-isolated peaks for each NV center are labeled as A, B, and C in Figure 1e. For these transitions, we repeat the resonant imaging experiment, each time fitting the result with a Gaussian point-spread function. The standard error on the fit centers gives a localization precision of $\langle S_A \rangle = 0.45$ nm for the brightest and most spectrally distinct NV [23]. Figure 1f shows the reconstructed positions, with spot widths indicating 10 times the localization precision after 40 minutes of integration and the dashed overlay showing the full-width half-maximum size of the original diffraction-limited spot.

We next consider the crosstalk that an optical readout of one NV induces in other NVs in a diffraction-limited spot. For simplicity, we first study these dynamics in a simple spin-1 system associated with a single NV center (NV_D) in site 2 of Figure 1c, which is initialized into state $|\psi_0\rangle = |m_s = 0\rangle + |m_s = 1\rangle$. Suppose a laser is applied at frequency ω_L for time T to perform resonant read-

* These two authors contributed equally.

† Current address: Niels Bohr Institute, University of Copenhagen, Blegdamsvej 17, 2100 Copenhagen, Denmark

‡ englund@mit.edu

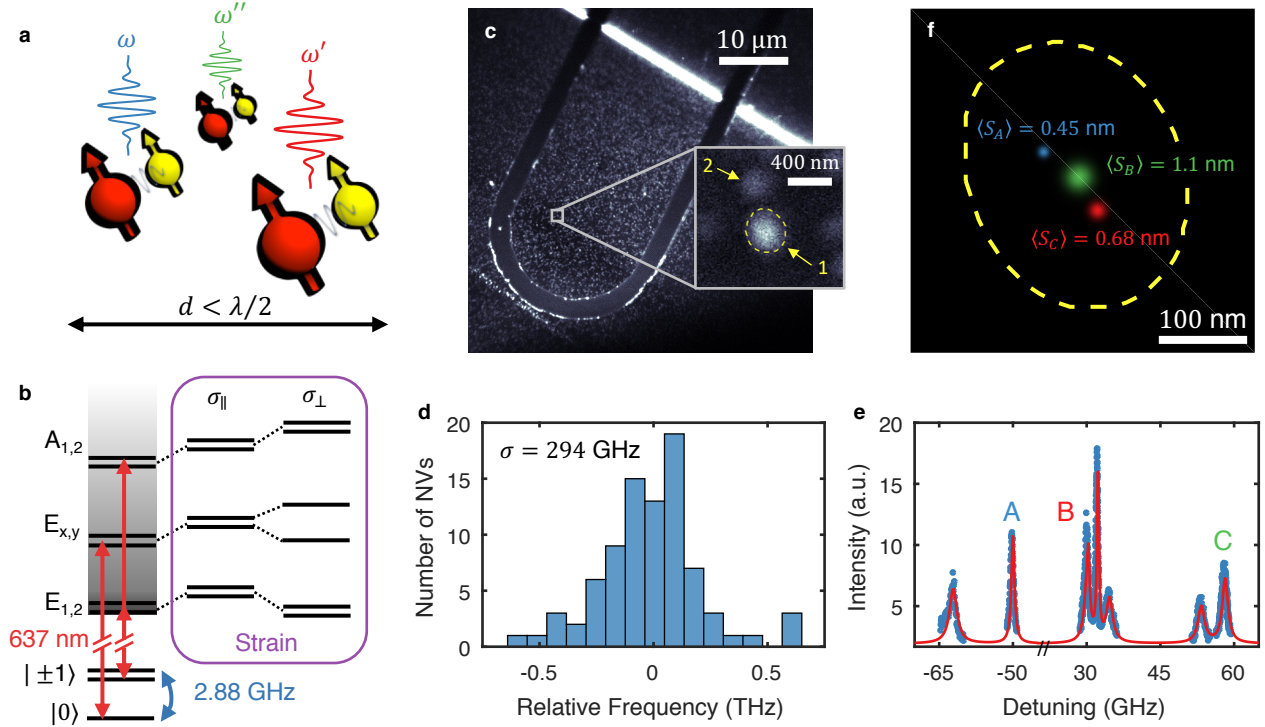


FIG. 1. **Preferential excitation and imaging of sub-diffraction defects.** **a**, An ensemble of NV electron spins (red) coupled to nearby nuclear spins (yellow) with distinct optical transition frequencies due to local strain fields, allowing selective interaction with individual centers operating on different frequency channels within a diffraction-limited spot. **b**, NV electron level structure. A ground state spin triplet acts as a qubit, addressable via 2.88 GHz microwave driving (blue). The spin-conserving radiative transitions (red) are at distinct frequencies, allowing optical spin readout via resonant excitation. Axial (σ_{\parallel}) and transverse (σ_{\perp}) strains shift these levels further and may distinguish individual NVs. **c**, Confocal microscope image of the PCD showing the microwave stripline. The bright white line is a grain boundary in the diamond. Inset, a close-up scan showing a brighter spot at site 1, determined to be a cluster of NVs, as well as a dimmer spot at site 2, determined to be a single NV. **d**, Histogram ($N=87$) showing the inhomogeneous distribution of ZPL transitions measured via PLE in the PCD, with a standard deviation $\sigma = 294$ GHz. **e**, PLE on the NV cluster at site 1, showing multiple transitions from strain-split centers, fit to a sum of 7 Lorentzians (red). **f**, Reconstructed locations within the cluster, with width (standard deviation) indicating the standard distance error on each point, multiplied 10x for visibility. For comparison, the dashed line shows the full-width half-maximum size of the spot under 532 nm excitation.

out on a hypothetical neighboring NV. This laser non-resonantly excites NV_D from ground state $|i\rangle$ into excited state $|k\rangle$, projecting its state by spontaneous emission into ground state $|j\rangle$, where $i, j \in m_s = \{-1, 0, 1\}$ and $k \in \{E_1, E_2, E_x, E_y, A_1, A_2\}$, with probability [23]:

$$\Gamma_{ijk} = 1 - \exp\left(-\frac{\gamma_{jk}\Omega_{ij}^2 T}{2(\Omega_{ij}^2 + \Delta_{ij}^2)}\right), \quad (1)$$

where Δ_{ij} is the detuning of ω_L from NV_D 's $|i\rangle \rightarrow |j\rangle$ ground-to-excited state transition, Ω_{ij} is the optical Rabi frequency, and γ_{jk} is the excited state's decay rate into $|k\rangle$. In addition to such a spontaneous-emission-induced state projection, NV_D may also acquire a phase shift due to the AC-Stark shift of the applied laser; however,

this is a weak and coherent process and can be compensated [23].

We probe this laser-induced crosstalk using Ramsey interferometry, as illustrated in Figure 2a. The application of an off-resonant laser (detuned by Δ from NV_D 's E_x transition) for fixed time T during the free precession period τ projects the NV into the mixed state:

$$\rho = (1 - \Gamma) |\psi\rangle\langle\psi| + \sum_k \left(\sum_{ij} \Gamma_{ijk} |k\rangle\langle k| \right), \quad (2)$$

where $|\psi\rangle = \frac{1}{\sqrt{2}} (|0\rangle + e^{-i\theta(t)} |1\rangle)$ is the result of the Ramsey experiment and $\sum \Gamma_{ijk} = \Gamma$. In our experiment, the excitation parameters and branching ratios are such

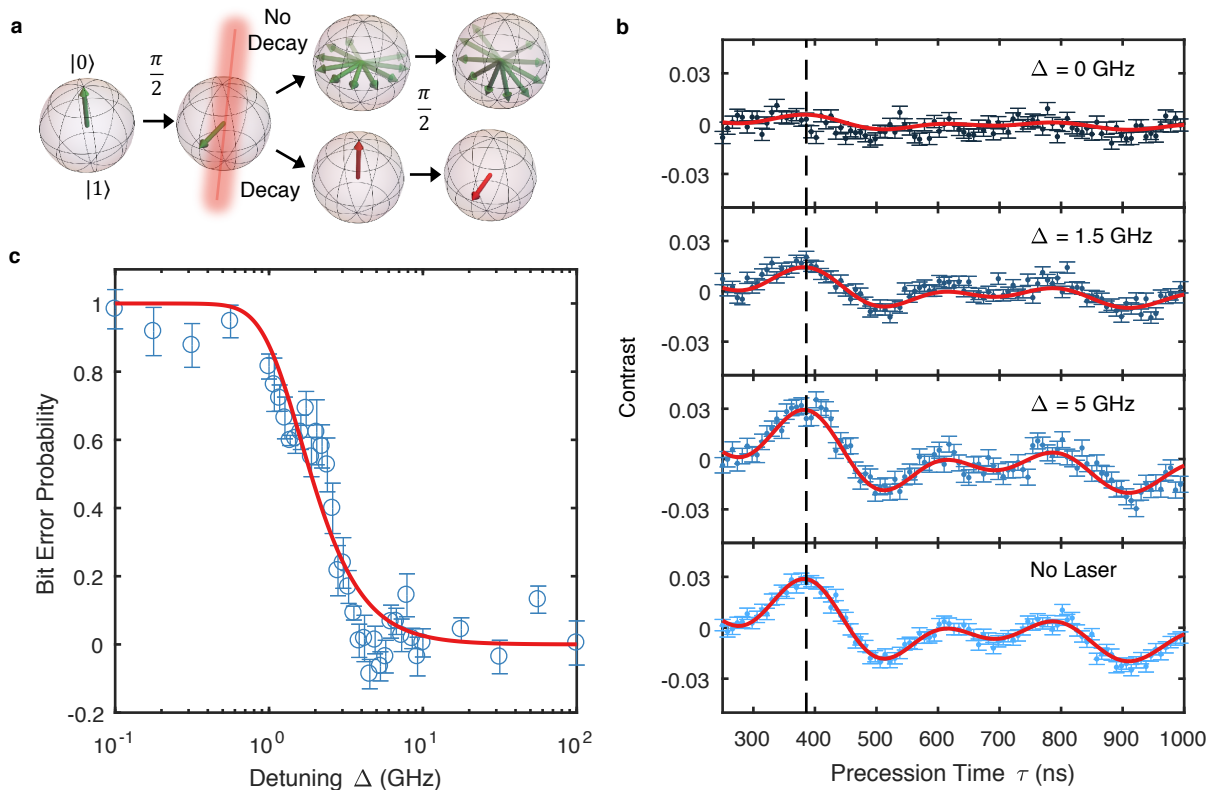


FIG. 2. **Qubit degradation under near-resonant excitation for a single isolated NV.** **a**, Bloch sphere schematic for crosstalk measurement sequence. After a $\pi/2$ -pulse prepares the qubit in a superposition state, it precesses around the Bloch sphere during application of a near-resonant laser. With probability $(1 - \Gamma)$, the laser will not induce excitation and subsequent decay, preserving the phase built up during the precession period, which is then mapped into population by a second $\pi/2$ -pulse and read out with a non-resonant readout pulse. However, the laser may also induce a spin-projecting decay event; in this scenario, the second $\pi/2$ -pulse will always place the spin in an even superposition state, independent of any phase accumulated during the precessory period, leading to a precession time-independent intensity at the final readout. **b**, Ramsey sequences with a resonant laser of varying detunings applied during the free precession period. The fits (solid lines) have one fit parameter for the fringe amplitude relative to that of a reference Ramsey taken with no crosstalk laser. **c**, Crosstalk probability as a function of laser detuning, taken by fixing the precession time to the fringe maximum at $\tau = 386$ ns (dashed line in **b**) and sweeping the resonant laser detuning. The contrast values are normalized to the fringe amplitude from the no-laser case. In red, the model for Γ (Eq. 1) with one fit parameter for the optical Rabi frequency.

that $\Gamma_{0,E_x,0}$ dominates the decay. The summed terms in Equation 2 are stationary states and provide no contrast in the Ramsey experiment, such that the fringe amplitude is directly proportional to $1 - \Gamma$. The final spin state (after the second $\pi/2$ -pulse of the Ramsey sequence) is measured by state-dependent fluorescence F through 532 nm illumination. F is normalized to account for power fluctuations by repeating the sequence, but replacing the final $\pi/2$ -gate with a $3\pi/2$ -gate and taking the contrast $C = \frac{(F_{3\pi/2} - F_{\pi/2})}{(F_{3\pi/2} + F_{\pi/2})}$.

Figure 2b plots C for varying Δ . For $\Delta = 0$, the Ramsey contrast vanishes, as expected for the laser-induced state projection. With increasing detuning, the fringe contrast recovers, approaching a control experiment without readout laser.

We map the crosstalk as a function of Δ by fixing the precession time to the fringe maximum at 386 ns and

sweeping the resonant laser over a wide range of detunings. These data are converted to a bit error probability in Figure 2c by normalizing the fluorescence from each detuning to that from the reference “no-laser” control experiment (Fig. 2b), which gives the crosstalk-free case. The red curve represents our model from Equation 1 with only one fit parameter for the optical Rabi frequency, which is difficult to accurately measure experimentally due to spectral diffusion of the ZPL. The optical excitation time T is fixed by our pulse generator, and the decay rate is determined by lifetime characterization [23]. The theory shows good agreement with our data and indicates that a detuning of 16 GHz or greater keeps crosstalk errors below 1%, a regime accessible by the cluster at site 1 of Figure 1c.

We now demonstrate individual control and readout on this cluster. We achieve independent microwave control

of the spin states by applying a magnetic field which splits the spin levels depending on the NV center crystal orientation. In this cluster, we find that two of the NV centers (A and B) are oriented along one crystal axis and the third (C) along another, indicated by four dips in the magnetic resonance spectrum [23].

We take advantage of this ground state splitting and apply the same Ramsey sequence from above to perform individual control and readout. Figure 3a shows the gate representation of our sequence. After initialization of all three NV centers with a 532 nm repump, the spin of NV C is coherently driven with a resonant microwave pulse

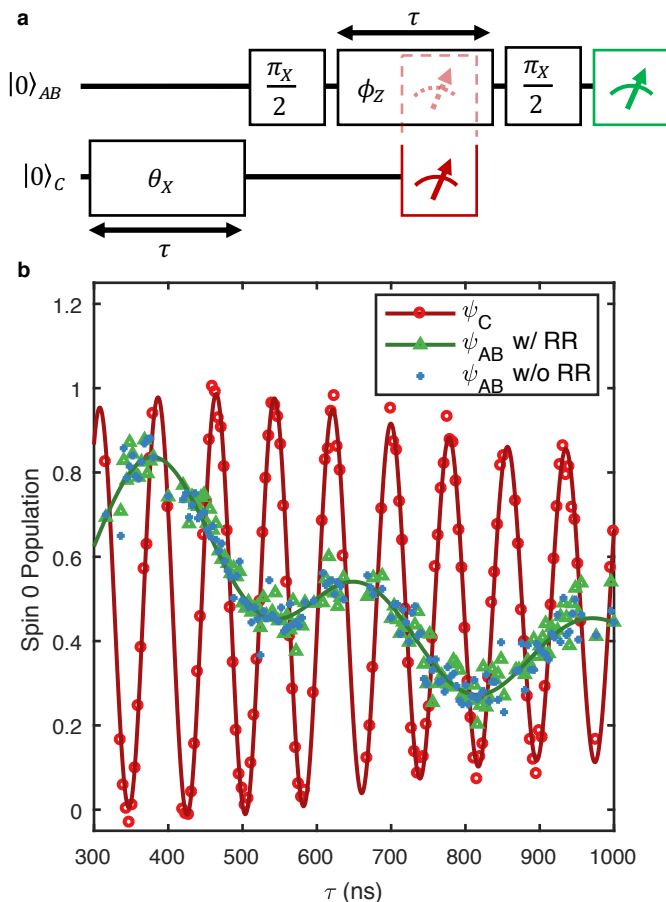


FIG. 3. **Simultaneous control and readout of three NVs in a sub-diffraction volume.** **a**, Gate sequence for demonstrating simultaneous control and readout of multiple NVs. A Rabi sequence is performed on NV C, followed by a subsequent Ramsey sequence on NVs A and B. During the Ramsey sequence, the state of NV C is read out using resonant readout (RR). The RR gate is depicted as partially spilling into $|\psi\rangle_{AB}$ to indicate the possibility of crosstalk. **b**, Results of the sequence in **a**, showing Rabi oscillations on NV C (red circles) and Ramsey fringes for NVs A and B (green triangles), alongside the reference Ramsey fringes (blue diamonds) for NVs A and B taken with no Rabi sequence nor RR on NV C. The green fit to the data for $|\psi\rangle_{AB}$ indicates no signal degradation within measurement error bounds [23].

for a time τ , inducing Rabi oscillations corresponding to a rotation of angle θ about the X -axis. Next, NVs A and B are rotated into an equal superposition state by a $\pi/2$ -pulse, followed by a passive precession by angle ϕ about the Z -axis for the same time τ . While NVs A and B are in this phase-sensitive superposition state, we perform individual readout on NV C using a resonant optical pulse. After waiting a total precession time τ , a final $\pi/2$ -pulse completes the Ramsey sequence on NVs A and B, and we read out these states with 532 nm light [23]. Note that while limitations in the available equipment necessitated the use of a non-resonant green readout on NVs A and B, additional lasers or modulators would allow for individual readout of each NV center in the cluster. Figure 3b shows the results of each readout window, where both gates measure the expected Rabi and Ramsey signals. Comparing these Ramsey results to that of a control Ramsey experiment on NVs A and B taken with no additional control or readout sequences on NV C, the fringe amplitudes are equal within our noise bounds ($0 \pm 4\%$ bit error probability). That is, we find no detectable fringe amplitude degradation as a result of the resonant readout pulse, indicating that the states of the off-resonant NV centers are left unperturbed through this readout. This result is consistent with our model, which predicts a bit error probability of $\sim 1\%$, below the 4% fit bounds.

We assess the viability of this platform for scalable creation of multi-spin registers by considering the probability of forming systems of multiple distinguishable emitters. Figure 4a shows the inhomogeneous distribution of NV center ZPL frequencies acquired on a single-crystal diamond (SCD, see Methods) from a dataset of 406 ZPL transitions from 197 distinct emitter sites. We consider here an SCD to allow comparison to samples most typically used in diamond quantum information experiments [4, 13, 24]. From this distribution, we build an empirical kernel estimate (red curve, Figure 4a).

Based on Monte Carlo sampling from this measured distribution, we estimate the probability that N emitters in a cluster have a crosstalk probability $\leq \Gamma$ under the parameters used for our multi-shot readout (MSR) in Figure 2. These results are given in Figure 4b. For example, the probability for an $N = 3$ NV site to have a crosstalk $\Gamma \leq 10^{-2}$ is estimated at 21%. If each of the NVs were coupled to 3 nuclear spin data qubits, such an $N = 3$ system would be sufficient for implementing the $[[9,1,3]]$ Shor-Bacon code [26].

Improved light collection using photonic microstructuring and single-shot readout (SSR) [25] could markedly improve these yields. To this end, we repeat our simulation under experimental parameters ($\Omega = \gamma$, $T = 3.7 \mu\text{s}$) comparable to those used to achieve single shot readout with 97% fidelity in a solid immersion lens [24]. The results in Figure 4c indicate a twofold increase in the $N = 3$ yield discussed above. Keeping these readout parameters and additionally assuming the measured ZPL distribution for the PCD (Figure 1d) produces the yield

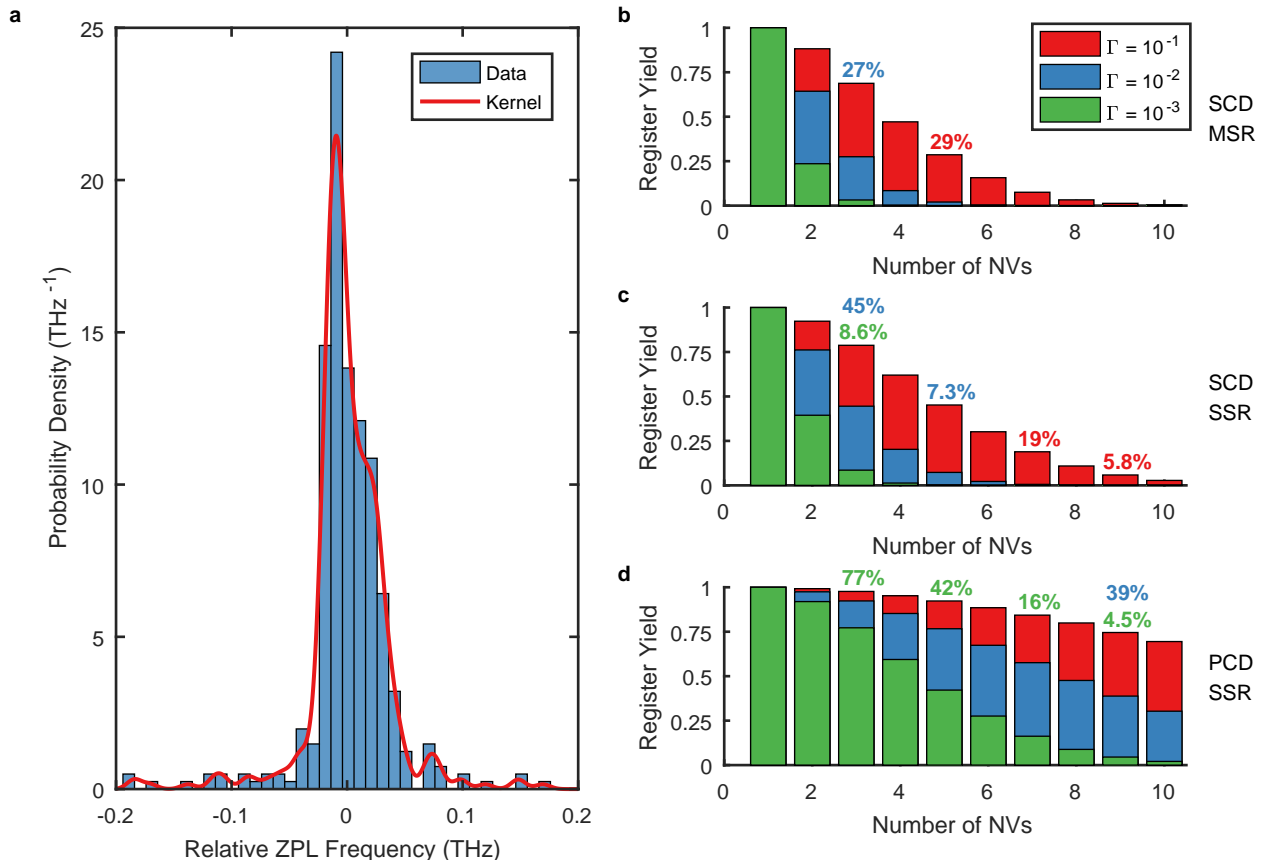


FIG. 4. **Architecture scalability.** **a**, Histogram (blue bars) of 406 zero-phonon line (ZPL) resonance frequencies normalized to be in units of probability density, and corresponding kernel density estimate (red line) of this inhomogeneous distribution. **b-d**, Simulated probabilities of successfully creating viable registers of varying numbers of NVs under different tolerance thresholds for the probability Γ of undesired spontaneous decays from off-resonant NVs. **b**, Results using MSR parameters shown in this work and the low-strain SCD distribution in **a**. **c**, Results using parameters used to demonstrate high-fidelity SSR [24, 25] and the low-strain SCD distribution in **a**. **d**, Results using single-shot readout parameters and the high-strain distribution measured in the PCD sample from Fig. 1–3.

histogram in Figure 4d, which shows that registers with $N = 9$ NVs could be produced with 39% yield with $\Gamma \leq 10^{-2}$.

In conclusion, we demonstrated readout of individual solid-state qubits within a diffraction-limited cluster with crosstalk on non-addressed qubits below 4×10^{-2} . This capability was enabled by strain-splitting of the NV centers’ ZPL transitions in a PCD. While this work uses native strain, the strain field may also be engineered [27] to provide greater control and increase inhomogeneous distributions. If an application necessitates a low-strain environment, these resonances can also be shifted by applying a DC electric field, allowing defects of different orientations — or the same orientation under a strong field gradient — to be uniquely addressed. The approach presented here is also applicable to other atom-like emitters, such as quantum dots [28], rare-earth ions [29], and other solid-state color centers. When combined with ex-

isting techniques for producing sub-diffraction clusters via aperture implantation [30], entangling defect centers with ancilla nuclear spins [17], and single-shot readout [25], this provides a path towards creating large ensembles of individually-addressable qubits, with a number of applications. For example, error-corrected registers using the 7-qubit [31] or 9-qubit [26] codes could be constructed with clusters of multiple coupled NV-dark spin systems, with full connectivity given by spin-spin coupling between adjacent NV centers. This would allow extension of architectures comprising one optically active and multiple dark spins [17] by reducing the problem of spectral crowding, as well as increasing the effective gate rate by parallelization. NV clusters with individual readout could also enable entanglement-assisted and spatially-resolved nanoscopic quantum sensing [2]. Finally, such clusters present an appealing architecture for modular quantum computing schemes [32, 33] and

spectrally-multiplexed quantum repeaters [15].

METHODS

Sample preparation

Super-resolution localization and individual control experiments were performed on a Type IIa PCD by chemical vapor deposition (Element 6), with a native nitrogen concentration of <50 ppb. To increase the prevalence of sub-diffraction clusters, the sample was implanted with nitrogen at 85 keV with a density of 10^{10} cm^{-2} , and subsequently annealed at 1200° C for 8 hours. The conversion yield of this process is on the order of 1%, resulting in a final areal NV density of roughly $1 \mu\text{m}^{-2}$. For delivering microwaves, striplines of 100 nm thick gold with a 5 nm titanium adhesion layer were fabricated via lift-off on the diamond surface. The single crystal Type IIa diamond was also produced by chemical vapor deposition (Element 6), with a native nitrogen concentration of <5 ppb. NV centers in this sample were created by implanting nitrogen (energy 185 eV, dosage 10^9 cm^{-2})

and subsequently annealing at 1200° C for 8 hours.

Experimental set-up

Experiments were performed using a home-built scanning confocal microscope. The samples were cooled to 4 K using a closed-cycle helium cryostat (Montana Instruments) and were imaged through a 0.9 NA vacuum objective. 532 nm light was generated by a Coherent Verdi G5 laser, and resonant red light tunable around 637 nm was generated by a New Focus Velocity tunable diode laser. Microwave signals were generated by Rohde & Schwarz SMIQ06B and SMV03 signal generators and sent through a high-power amplifier (Mini-Circuits ZHL-16W-43+) before delivery to the sample.

Data availability

The data that support the plots within this paper and other findings of this study are available from the corresponding author upon reasonable request.

-
- [1] John Preskill, “Quantum computing in the nisq era and beyond,” (2018), arXiv:1801.00862.
- [2] C. L. Degen, F. Reinhard, and P. Cappellaro, “Quantum sensing,” *Rev. Mod. Phys.* **89**, 035002 (2017).
- [3] J. Zhang, P. W. Hess, A. Kyprianidis, P. Becker, A. Lee, J. Smith, G. Pagano, I. D. Potirniche, A. C. Potter, A. Vishwanath, N. Y. Yao, and C. Monroe, “Observation of a discrete time crystal,” *Nature* **543**, 217 (2017).
- [4] Soonwon Choi, Joonhee Choi, Renate Landig, Georg Kucsko, Hengyun Zhou, Junichi Isoya, Fedor Jelezko, Shinobu Onoda, Hitoshi Sumiya, Vedika Khemani, Curt von Keyserlingk, Norman Y. Yao, Eugene Demler, and Mikhail D. Lukin, “Observation of discrete time-crystalline order in a disordered dipolar many-body system,” *Nature* **543**, 221 (2017).
- [5] M. Hamed Mohammady, Hyeonrak Choi, Matthew E. Trusheim, Abolfazl Bayat, Dirk Englund, and Yasser Omar, “Low-control and robust quantum refrigerator and applications with electronic spins in diamond,” *Phys. Rev. A* **97**, 042124 (2018).
- [6] W. B. Gao, A. Imamoglu, H. Bernien, and R. Hanson, “Coherent manipulation, measurement and entanglement of individual solid-state spins using optical fields,” *Nature Photonics* **9**, 363 (2015).
- [7] Peter C. Humphreys, Norbert Kalb, Jaco P. J. Morits, Raymond N. Schouten, Raymond F. L. Vermeulen, Daniel J. Twitchen, Matthew Markham, and Ronald Hanson, “Deterministic delivery of remote entanglement on a quantum network,” *Nature* **558**, 268–273 (2018).
- [8] F. Dolde, I. Jakobi, B. Naydenov, N. Zhao, S. Pezzagna, C. Trautmann, J. Meijer, P. Neumann, F. Jelezko, and J. Wrachtrup, “Room-temperature entanglement between single defect spins in diamond,” *Nature Physics* **9**, 139 (2013).
- [9] Edward H. Chen, Ophir Gaathon, Matthew E. Trusheim, and Dirk Englund, “Wide-field multispectral super-resolution imaging using spin-dependent fluorescence in nanodiamonds,” *Nano Letters* **13**, 2073–2077 (2013).
- [10] Jean-Christophe Jaskula, Erik Bauch, Silvia Arroyo-Camejo, Mikhail D. Lukin, Stefan W. Hell, Alexei S. Trifonov, and Ronald L. Walsworth, “Superresolution optical magnetic imaging and spectroscopy using individual electronic spins in diamond,” *Opt. Express* **25**, 11048–11064 (2017).
- [11] Marcus W. Doherty, Neil B. Manson, Paul Delaney, Fedor Jelezko, Jrg Wrachtrup, and Lloyd C.L. Hollenberg, “The nitrogen-vacancy colour centre in diamond,” *Physics Reports* **528**, 1 – 45 (2013).
- [12] Tohru Tanaka, Paul Knott, Yuichiro Matsuzaki, Shane Dooley, Hiroshi Yamaguchi, William J. Munro, and Shiro Saito, “Proposed robust entanglement-based magnetic field sensor beyond the standard quantum limit,” *Phys. Rev. Lett.* **115**, 170801 (2015).
- [13] G. Waldherr, Y. Wang, S. Zaiser, M. Jamali, T. Schulte-Herbruggen, H. Abe, T. Ohshima, J. Isoya, J. F. Du, P. Neumann, and J. Wrachtrup, “Quantum error correction in a solid-state hybrid spin register,” *Nature* **506**, 204–207 (2014).
- [14] J. Cramer, N. Kalb, M. A. Rol, B. Hensen, M. S. Blok, M. Markham, D. J. Twitchen, R. Hanson, and T. H. Taminiau, “Repeated quantum error correction on a continuously encoded qubit by real-time feedback,” *Nature Communications* **7**, 11526 (2016).
- [15] Neil Sinclair, Erhan Saglamyurek, Hassan Mallahzadeh, Joshua A. Slater, Mathew George, Raimund Ricken, Morgan P. Hedges, Daniel Oblak, Christoph Simon, Wolfgang Sohler, and Wolfgang Tittel, “Spectral multiplexing for scalable quantum photonics using an atomic

- frequency comb quantum memory and feed-forward control,” *Phys. Rev. Lett.* **113**, 053603 (2014).
- [16] Suzanne B van Dam, Peter C Humphreys, Filip Rozpdek, Stephanie Wehner, and Ronald Hanson, “Multiplexed entanglement generation over quantum networks using multi-qubit nodes,” *Quantum Science and Technology* **2**, 034002 (2017).
- [17] M. H. Abobeih, J. Cramer, M. A. Bakker, N. Kalb, M. Markham, D. J. Twitchen, and T. H. Taminiau, “One-second coherence for a single electron spin coupled to a multi-qubit nuclear-spin environment,” *Nature Communications* **9**, 2552 (2018).
- [18] E. L. Rosenfeld, L. M. Pham, M. D. Lukin, and R. L. Walsworth, “Sensing coherent dynamics of electronic spin clusters in solids,” *Phys. Rev. Lett.* **120**, 243604 (2018).
- [19] Hannes Bernien, Lilian Childress, Lucio Robledo, Matthew Markham, Daniel Twitchen, and Ronald Hanson, “Two-photon quantum interference from separate nitrogen vacancy centers in diamond,” *Phys. Rev. Lett.* **108**, 043604 (2012).
- [20] A. Sipahigil, K. D. Jahnke, L. J. Rogers, T. Teraji, J. Isoya, A. S. Zibrov, F. Jelezko, and M. D. Lukin, “Indistinguishable photons from separated silicon-vacancy centers in diamond,” *Phys. Rev. Lett.* **113**, 113602 (2014).
- [21] M W Doherty, N B Manson, P Delaney, and L C L Hollenberg, “The negatively charged nitrogen-vacancy centre in diamond: the electronic solution,” *New Journal of Physics* **13**, 025019 (2011).
- [22] Matthew E Trusheim and Dirk Englund, “Wide-field strain imaging with preferentially aligned nitrogen-vacancy centers in polycrystalline diamond,” *New Journal of Physics* **18**, 123023 (2016).
- [23] See Supplementary Information for additional derivations, data, and analysis.
- [24] B. Hensen, H. Bernien, A. E. Dréau, A. Reiserer, N. Kalb, M. S. Blok, J. Ruitenbergh, R. F. L. Vermeulen, R. N. Schouten, C. Abellán, W. Amaya, V. Pruneri, M. W. Mitchell, M. Markham, D. J. Twitchen, D. Elkouss, S. Wehner, T. H. Taminiau, and R. Hanson, “Loophole-free bell inequality violation using electron spins separated by 1.3 kilometres,” *Nature* **526**, 682 (2015).
- [25] Lucio Robledo, Lilian Childress, Hannes Bernien, Bas Hensen, Paul F. A. Alkemade, and Ronald Hanson, “High-fidelity projective read-out of a solid-state spin quantum register,” *Nature* **477**, 574 (2011).
- [26] Dave Bacon, “Operator quantum error-correcting subsystems for self-correcting quantum memories,” *Phys. Rev. A* **73**, 012340 (2006).
- [27] Srujan Meesala, Young-Ik Sohn, Benjamin Pingault, Linbo Shao, Haig A. Atikian, Jeffrey Holzgrafe, Mustafa Gündoğan, Camille Stavrakas, Alp Sipahigil, Cleaven Chia, Ruffin Evans, Michael J. Burek, Mian Zhang, Lue Wu, Jose L. Pacheco, John Abraham, Edward Bielejec, Mikhail D. Lukin, Mete Atatüre, and Marko Lončar, “Strain engineering of the silicon-vacancy center in diamond,” *Phys. Rev. B* **97**, 205444 (2018).
- [28] David Press, Thaddeus D. Ladd, Bingyang Zhang, and Yoshihisa Yamamoto, “Complete quantum control of a single quantum dot spin using ultrafast optical pulses,” *Nature* **456**, 218 (2008).
- [29] A. M. Dibos, M. Raha, C. M. Phenicie, and J. D. Thompson, “Atomic source of single photons in the telecom band,” *Phys. Rev. Lett.* **120**, 243601 (2018).
- [30] I Jakobi, S A Momenzadeh, F Fvaro de Oliveira, J Michl, F Ziem, M Schreck, P Neumann, A Denisenko, and J Wrachtrup, “Efficient creation of dipolar coupled nitrogen-vacancy spin qubits in diamond,” *Journal of Physics: Conference Series* **752**, 012001 (2016).
- [31] A. M. Steane, “Error correcting codes in quantum theory,” *Phys. Rev. Lett.* **77**, 793–797 (1996).
- [32] Naomi H. Nickerson, Joseph F. Fitzsimons, and Simon C. Benjamin, “Freely scalable quantum technologies using cells of 5-to-50 qubits with very lossy and noisy photonic links,” *Phys. Rev. X* **4**, 041041 (2014).
- [33] Mihir Pant, Hyeonrak Choi, Saikat Guha, and Dirk Englund, “Percolation based architecture for cluster state creation using photon-mediated entanglement between atomic memories,” (2017), arXiv:1704.07292.

ACKNOWLEDGEMENTS

E.B. was supported by a NASA Space Technology Research Fellowship and the NSF Center for Ultracold Atoms (CUA). M.W. was supported by the STC Center for Integrated Quantum Materials (CIQM), NSF Grant No. DMR-1231319, the Army Research Laboratory Center for Distributed Quantum Information (CDQI), and Master Dynamic Limited. S.L.M. was supported by the NSF EFRI-ACQUIRE program Scalable Quantum Communications with Error-Corrected Semiconductor Qubits and the AFOSR Quantum Memories MURI. M.E.T. was supported by an appointment to the Intelligence Community Postdoctoral Research Fellowship Program at MIT, administered by Oak Ridge Institute for Science and Education through an interagency agreement between the U.S. Department of Energy and the Office of the Director of National Intelligence. T.S. was supported by the European Unions Horizon 2020 research and innovation programme under the Marie Skłodowska-Curie grant agreement no. 753067 (OPHOCS). This work was supported in part by the AFOSR MURI for Optimal Measurements for Scalable Quantum Technologies (FA9550-14-1-0052) and by the AFOSR program FA9550-16-1-0391, supervised by Gernot Pomrenke. The authors would like to thank C. Foy, H. Choi, and C. Peng for helpful discussions.

AUTHOR CONTRIBUTIONS

E.B. and M.W. performed the experiments. E.B. and T.S. constructed the optical setup. S.L.M., M.E.T., and M.W. prepared the sample. E.B., M.W., M.E.T., T.S., and D.R.E. conceived the experiments. E.B., M.W., S.L.M., and D.R.E. prepared the manuscript. All authors reviewed the manuscript.

COMPETING FINANCIAL INTERESTS

The authors declare no competing financial interests.